

Direct Numerical Simulation of Anisotropic Particles in Turbulent Flow

by  
Kai Roberts

A THESIS

submitted to  
Oregon State University  
Honors College

in partial fulfillment of  
the requirements for the  
degree of

Honors Baccalaureate of Science in Mechanical Engineering  
(Honors Scholar)

Presented June 1, 2021  
Commencement June 2021



## AN ABSTRACT OF THE THESIS OF

Kai Roberts for the degree of Honors Baccalaureate of Science in Mechanical Engineering presented on June 1, 2021. Title: Direct Numerical Simulation of Anisotropic Particles in Turbulent Flow.

Abstract approved: \_\_\_\_\_

Sourabh V. Apte

Turbulent flows with suspended, non-spherical particles are common in many natural and industrial processes. To identify the effects of anisotropic geometry on particle dynamics, a one-way coupled Lagrangian direct numerical simulation solver was written, verified, and used to collect data on particles simulated in multiple flows. This thesis explains the methods used to develop an anisotropic particle flow solver and explores the behaviors of the simulated particles. The dynamics of prolate ellipsoidal particles with aspect ratios between 1.001 and 25 were simulated in two-dimensional laminar Taylor-Green vortex flow and in a three-dimensional turbulent flow. During these simulations particle mass and particle density were held constant. The following major trends were identified through simulation. In the laminar case, the particles tended to orient in the stream wise direction and settling orientation speed correlated with higher aspect ratios. The laminar case also showed minor change in translational velocity with changing aspect ratio. Particles with lower aspect ratios tended to have a lower average difference between the particle and fluid velocity. The three-dimensional turbulent flow showed that ellipsoidal particles quickly disperse based on aspect ratio but supports the same conclusions as the laminar two-dimensional case where rounder particles are traversed the domain faster.

Key Words: Anisotropic particles, Fibers, Preferential orientation, Ellipsoid

Corresponding e-mail address: robertk3@oregonstate.edu

©Copyright by Kai Roberts  
June 1, 2021

Direct Numerical Simulation of Anisotropic Particles in Turbulent Flow

by  
Kai Roberts

A THESIS

submitted to  
Oregon State University  
Honors College

in partial fulfillment of  
the requirements for the  
degree of

Honors Baccalaureate of Science in Mechanical Engineering  
(Honors Scholar)

Presented June 1, 2021  
Commencement June 2021

Honors Baccalaureate of Science in Mechanical Engineering project of Kai Roberts  
presented on June 1, 2021.

APPROVED:

---

Sourabh V. Apte, Mentor, representing School of Mechanical, Industrial, and Manufacturing  
Engineering

---

Gregory Wilson, Committee Member, representing College of Earth, Ocean, and  
Atmospheric Sciences

---

Ravi Balasubramanian, Committee Member, representing School of Mechanical, Industrial,  
and Manufacturing Engineering

---

Toni Doolen, Dean, Oregon State University Honors College

I understand that my project will become part of the permanent collection of Oregon State  
University, Honors College. My signature below authorizes release of my project to any  
reader upon request.

---

Kai Roberts, Author



## 1. Introduction

### 1.1 Background

Turbulent flows with suspended, non-spherical particles are common in many natural and industrial processes. Some examples include fuel injection and soot emissions from combustion, cough droplets dispersed in the air of operating rooms, cloth fibers in industrial manufacturing, and pharmaceutical processes (*see Fig.1*). Some natural processes include modeling of plankton in the oceans and pollen in the atmosphere. These processes commonly have elongated rigid fiber like particles with anisotropic properties deriving from the non-spherical geometry. Computer simulation of these anisotropic particles in turbulent flow can be used to characterize the orientation and dynamics of the particles which is necessary for optimizing engineering designs for each application.

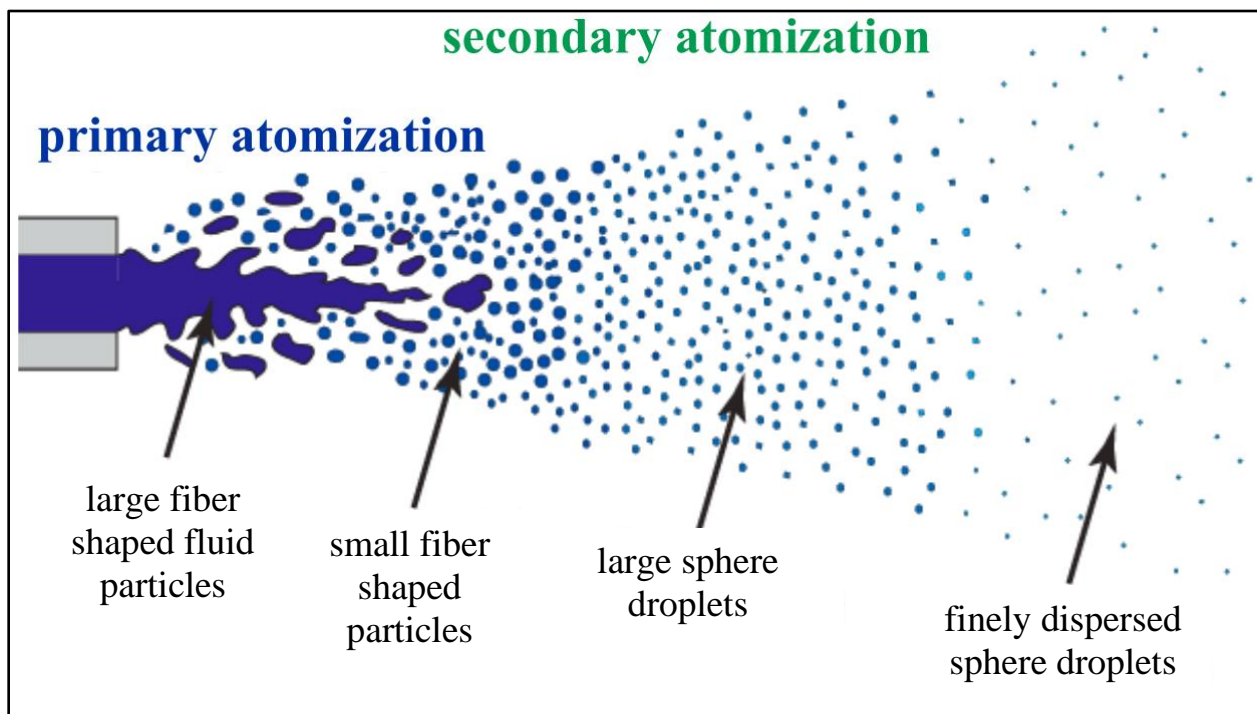


**Figure 1:** Evolution of droplet particle in a fuel injection process [1].

An exemplar case of anisotropic particles in turbulent flow is the atomization of fuel within engines during the fuel injection process. Figure 1 shows the particle evolution process from concentrated fiber shaped jets to finely dispersed droplets. Improved modeling of anisotropic particles can be

used to characterize the dispersion of fuel which can be used to inform the design process of fuel injectors and combustion chamber geometry.

Despite the common nature of anisotropic particle processes, typical simulations of multiphase fluid flows utilize spherical particles with isotropic properties to approximate the behavior of anisotropic particles. This reduces simulation certainty and removes the ability to calculate particle orientation dynamics. When compared to spherical particles, anisotropic particles exhibit many differing behaviors such as their orientation dynamics, concentration dynamics, and rotation dynamics because of the effects of anisotropic geometry on hydrodynamic drag and torque. Many of the parameters related to modeling anisotropic particles in turbulent flows are still unexplored and fluid dynamics is an ongoing field of research. While numerical modeling of spherical particles in turbulent flow is common and well understood, there is only a limited body of research regarding simulation of anisotropic particles in turbulent flow (*see Sec. 1.2*) and should be explored further [2]. This thesis explains the methods used to develop a solver capable of simulating anisotropic particle dynamics in flow with one way coupling to investigate the methods for developing a solver to compare the behavior of non-spherical particles to spherical particles in both two-dimensional laminar Taylor-Green vortex flow and in turbulent three-dimensional flow to characterize the effects of anisotropic geometry on particle dynamics. The simulation particles are coupled one way with the fluid effecting the particles only. This simplification is justified through the low particle volume ratio. The custom simulation model is verified through time step error quantification and validated through comparisons to known behaviors of spherical particles. The long-term goal of this work is to develop a robust methodology to simulate many anisotropic particles simultaneously in any flow conditions through integration with particle solvers such as that ran by the Computational Flow Physics Laboratory [3].

This paper is organized with the following structure. Section 2 explains the methods used in writing the particle dynamics solver by explaining the properties of the particle, flow fields, kinematic and dynamic equations of motion, the rotation framework, the program logic, and experimental parameters being tested. Section 3 describes some verification for the simulation through comparisons to known behaviors of particle dynamics. Section 4 explains the results gathered from

the experiment. Section 5 discusses the significance of the findings and proposes possible next steps to further this work.

## **1.2 Literature Review**

Research on particulate flows is largely concentrated on modeling spherical particles due to the computational requirements of implementing anisotropic calculations in flow solvers [4]. Despite this, research on ellipsoidal particles in fluid flows has been ongoing for several decades. Previously, rod like particles in turbulent flow have been experimentally analyzed by Parsheh and Paschewitz respectively [5, 6]. Parsheh, utilizing high speed imaging and laser-doppler velocimetry techniques have verified that the Fokker-Planck type equations are accurate to real life experimental results [5]. Likewise, Paschewitz also verified that a rigid rod constitutive equation based numerical scheme was accurate to experimental results [6]. Mathematic equations for the torques acting on ellipsoidal particles have been derived by Jeffery (1922), Brenner (1963, 1964), and Harper (1968) [7, 8, 9]. The Jeffery study from 1922 is the foundation of many modern ellipsoidal particle research through the derivation of hydrodynamic drag force and torque values for particle dynamics in creeping flow. Modern research toward ellipsoidal particles has trended toward numerical analysis and experimentation of ellipsoidal flows and has progressed toward four way coupling of ellipsoidal particles in turbulent flows. Notable findings include indications that fibers typically orient horizontally in atmospheric turbulence and that fiber orientation is more effected by fiber diameter than length [10]. Zhang in 2001 did a similar study of particles in turbulent channel flow and determined that particles congregate toward wall boundaries and orient in the streamwise direction [11]. This paper utilizes the Lagrangian particle dynamics equations developed by Brenner, the quaternion rotation framework developed by Zhao, and uses a similar computation loop as described by Zhang [8, 10, 11]. Future research in ellipsoidal particles would aims to fully resolve the effects of “forcing and boundary conditions, fluid density, fluid viscosity, particle size and shape, particle density, and particle concentration” as well as “the particle translational and rotational diffusivity, gravitational acceleration, particle deformability, collisions, aggregation or fragmentation, non-Newtonian fluid rheology, and electrostatic forces” [12].

## 2. Methods

To explore the effects of anisotropic geometry on particle behavior in flow, a solver was written using the methods presented in this section.

### 2.1 Ellipsoidal Particle Model

This analysis explores the behavior of rigid prolate ellipsoidal particles with equal semi-minor axis (see Fig. 2).

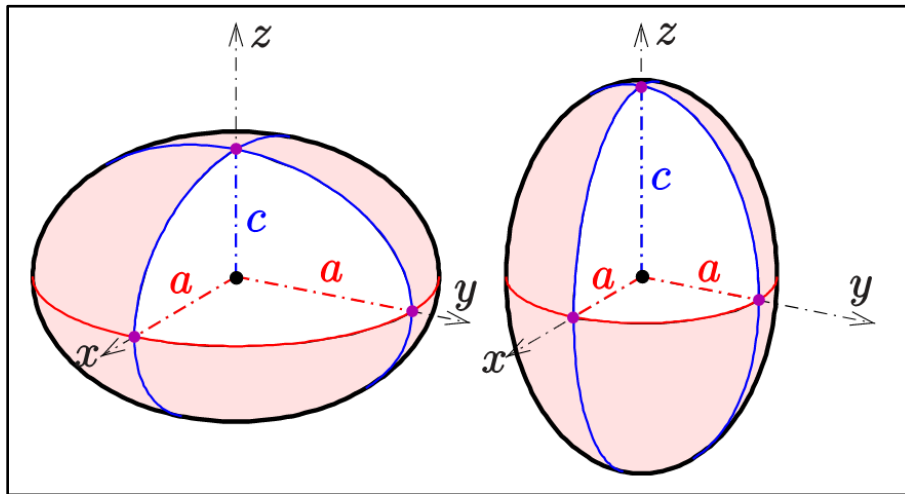


**Figure 2:** (Left) Diagram of an oblate spheroid with a larger semi-minor axis than semi-major axis. (Right) Diagram of a prolate spheroid with a larger semi-major axis than semi-minor axis [13].

The ellipsoid aspect ratio ( $\lambda$ ) is defined as  $\lambda = c/a$  where  $a$  is the semi-minor axis and  $c$  is the semi-major axis. The particle is further characterized by  $\rho_p$ , its particle density, which is used to calculate the mass of the particle ( $m$ ). The mass of the particle is calculated by the following equation:

$$m = \frac{4}{3} \pi a^2 c \lambda \rho_p \quad (\text{Eq. 1})$$

This analysis examines ellipsoids with a  $\rho_p$  of  $120 \text{ kg/m}^3$  and  $\lambda$  values between 0.001 and 25 (see Table 1).

## 2.2 Flow Model

### 2.2.1 Taylor-Green Vortex Flow

This work presents data from simulations using two flows. The first flow is Taylor-Green vortex flow which is a two-dimensional laminar decaying vortex flow that has an analytical solution in time and space (*see Fig. 3*). It is primarily used for validation of time-accurate problems due to its exact solution. The Taylor-Green vortex used in this simulation is defined within a square computational grid of length and height equal to  $2\text{ m}$ . The solution of the flow used in this thesis is as follows:

$$u_x(x, y, t) = -\cos(\pi x)\sin(\pi y)e^{-2\pi^2 vt} \quad (\text{Eq. 2})$$

$$u_y(x, y, t) = \sin(\pi x)\cos(\pi y)e^{-2\pi^2 vt} \quad (\text{Eq. 3})$$

$$p(x, y, t) = -0.25[\cos(2\pi x) + \cos(2\pi y)]e^{-4\pi^2 vt} \quad (\text{Eq. 4})$$

$$v = \mu/\rho_f \quad (\text{Eq. 5})$$

where  $(u_x, u_y, u_z)$  is the particle velocity vector components,  $(x, y, z)$  is the particle position components,  $t$  is the time of the simulation,  $p$  is the pressure,  $v$  is the kinematic viscosity,  $\mu$  is the dynamic viscosity, and  $\rho_f$  is the density of the fluid.

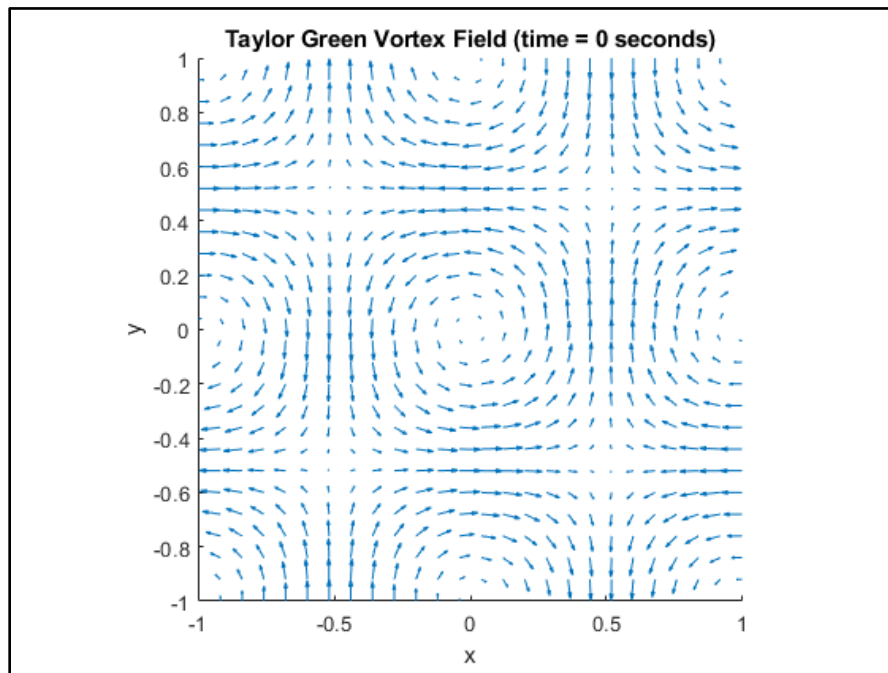


**Figure 3:** Instantaneous fluid velocity magnitude plot for 2D Taylor-Green vortex flow in a  $25 \times 25$  grid with axis of length  $2\text{ m}$ .

### 2.2.2 3D Isotropic Turbulence Flow Field

The second flow used in each simulation is a three-dimensional turbulent flow and is pictured in Figure 4. The second flow is used to test the solver for ellipsoid particles in turbulent flow with calculations made in three dimensions. The turbulent three-dimensional flow is generated by taking a snapshot of three-dimensional isotropic turbulence at a single point in time. The data is stored on a coarse  $64^3$  grid with equal spacing and side lengths of  $2\pi m$ . The flow has a Komogorov scale of 0.05. The fluid has a  $\rho_f = 1 \text{ kg/m}^3$  and a  $\mu = 0.0200008 \text{ Pa} \cdot \text{s}$ .

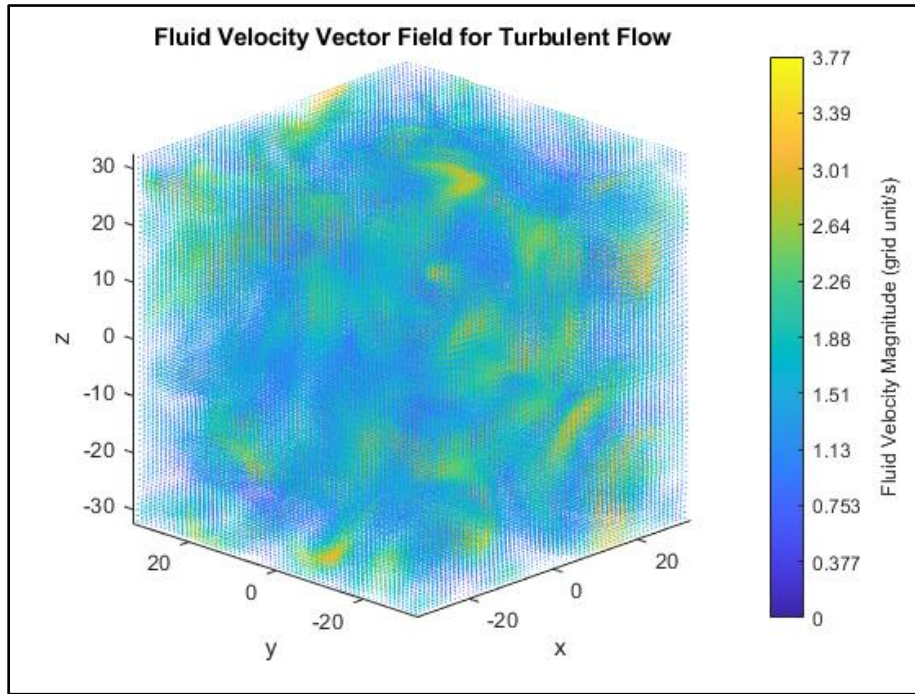


**Figure 4:** Instantaneous fluid velocity magnitude plot (indicated by color) for 3D turbulent flow in a  $63 \times 63 \times 63$  coarse grid with volume of  $2\pi m^3$ . Lighter colors denote greater fluid velocity magnitude.

The Eulerian fluid dynamics are governed by the continuity and Navier-Stokes equations, written for incompressible, isothermal, and Newtonian fluid.

$$\nabla \cdot u = 0 \quad (\text{Eq. 6})$$

$$\frac{\partial u}{\partial t} + u \cdot \nabla u = \nu \nabla^2 u - \frac{1}{\rho_f} \nabla P \quad (\text{Eq. 7})$$

### 2.3 Kinematics + Dynamics Methods

The translational motion of the particles is calculated using Newton's second law:

$$\sum F = m \frac{du_p}{dt} \quad (\text{Eq. 8})$$

where  $\sum F$  is a sum of the two significant hydrodynamic forces acting on the particle which are drag and gravity. The hydrodynamic drag force affecting the ellipsoid particles was evaluated by Brenner under creeping flow conditions as

$$F_{drag} = \mu^f \pi a K (u_{f@p} - u) \quad (\text{Eq. 9})$$

where  $F_{drag}$  is the hydrodynamic drag force and  $K$  is the resistance tensor evaluated in world space and  $u_{f@p}$  is the particle velocity vector evaluated at the centroid of the particle [7]. The resistance tensor is converted to world space using the following equation:

$$K = (q(qK^bq^{-1})^Tq^{-1})^T \quad (\text{Eq. 10})$$

$$K^b = \begin{bmatrix} K_{xx}^b & 0 & 0 \\ 0 & K_{yy}^b & 0 \\ 0 & 0 & K_{zz}^b \end{bmatrix} \quad (\text{Eq. 11})$$

where  $q$  is the quaternion of the particle (*see section 2.3.1*) and  $K^b$  is the resistance tensor evaluated in body space with the following components:

$$K_{xx}^b = \frac{8(\lambda^2 - 1)^{3/2}}{(2\lambda^2 - 1)\ln(\lambda + \sqrt{\lambda^2 - 1}) - \lambda(\sqrt{\lambda^2 - 1})} \quad (\text{Eq. 12})$$

$$K_{yy}^b = K_{zz}^b = \frac{16(\lambda^2 - 1)^{3/2}}{(2\lambda^2 - 3)\ln(\lambda + \sqrt{\lambda^2 - 1}) + \lambda(\sqrt{\lambda^2 - 1})} \quad (\text{Eq. 13})$$

The second component of  $\sum F$  is the gravity force which is calculated by:

$$F_{gravity} = (\rho_p - \rho_f) * m * g \quad (\text{Eq. 14})$$

where  $g$  is an acceleration vector with a z component of  $-9.81 \text{ m/s}$ .

The angular acceleration of the ellipsoidal particles comes from hydrodynamic torques applied to the particle. To calculate this, the acceleration of angular momentum equation of particles is used:

$$\dot{\omega}^b = (I^b)^{-1}(N^b - \omega^b \times I^b \omega^b) \quad (\text{Eq. 15})$$

where  $\dot{\omega}^b$  is the angular acceleration of the particle in body space,  $\omega^b$  is the angular velocity of the particle,  $I^b$  is the inertia tensor of the particle, and  $N^b$  is the total torque acting on the particle.

The superscript  $b$  denotes variables evaluated in the body space (*see Section 2.3.1*). The inertia tensor of prolate spheroids in body space is calculated using the following equations:

$$I^b = \begin{bmatrix} I_{xx}^b & 0 & 0 \\ 0 & I_{yy}^b & 0 \\ 0 & 0 & I_{zz}^b \end{bmatrix} \quad (\text{Eq. 16})$$

$$I_{xx}^b = \frac{2ma^2}{5} \quad (\text{Eq. 17})$$

$$I_{yy}^b = I_{zz}^b = \frac{(1 + \lambda^2)ma^2}{5} \quad (\text{Eq. 18})$$

The total torque acting on the particle is calculated by:

$$N^b = \begin{bmatrix} N_x^{b,h} \\ N_y^{b,h} \\ N_z^{b,h} \end{bmatrix} \quad (\text{Eq. 19})$$

$$N_x^{b,h} = \frac{32\pi\mu^f a^3 \lambda}{3(\alpha_2 + \alpha_3)} (\Omega_{zy}^b - \omega_x^b) \quad (\text{Eq. 20})$$

$$N_y^{b,h} = \frac{16\pi\mu^f a^3 \lambda}{3(\alpha_3 + \lambda^2 \alpha_1)} ((1 - \lambda^2)S_{xz}^b + (1 + \lambda^2)(\Omega_{xz}^b - \omega_y^b)) \quad (\text{Eq. 21})$$

$$N_z^{b,h} = \frac{16\pi\mu^f a^3 \lambda}{3(\alpha_2 + \lambda^2 \alpha_1)} ((1 - \lambda^2)S_{yx}^b + (1 + \lambda^2)(\Omega_{yx}^b - \omega_z^b)) \quad (\text{Eq. 22})$$

where the  $S_{i,j}^b$  and  $\Omega_{i,j}^b$  represent the fluid strain rate tensor and the rotation tensor in body space.

They are calculated using the following:

$$S_{i,j}^b = \frac{1}{2} \left( \frac{\partial u_i^{fb}}{\partial x_j} + \frac{\partial u_j^{fb}}{\partial x_i} \right) \quad (\text{Eq. 23})$$

$$\Omega_{i,j}^b = \frac{1}{2} \left( \frac{\partial u_i^{fb}}{\partial x_j} - \frac{\partial u_j^{fb}}{\partial x_i} \right) \quad (\text{Eq. 24})$$

The constants  $\alpha_1$ ,  $\alpha_2$ , and  $\alpha_3$  are defined by:

$$\alpha_1 = -\frac{2}{\lambda^2 - 1} - \frac{\lambda}{(\lambda^2 - 1)^{3/2}} \ln \left[ \frac{\lambda - (\lambda^2 - 1)^{1/2}}{\lambda + (\lambda^2 - 1)^{1/2}} \right] \quad (\text{Eq. 25})$$

$$\alpha_2 = \alpha_3 = \frac{2}{\lambda^2 - 1} + \frac{\lambda}{2(\lambda^2 - 1)^{3/2}} \ln \left[ \frac{\lambda - (\lambda^2 - 1)^{1/2}}{\lambda + (\lambda^2 - 1)^{1/2}} \right] \quad (\text{Eq. 26})$$

### 2.3.1 Rotation Framework

To capture the Lagrangian motion of each particle two primary coordinate systems are used. The body space coordinate axis and the world space coordinate axis are presented in Figure 5 alongside an illustration of the Euler axis used to calculate the quaternion of each particle.

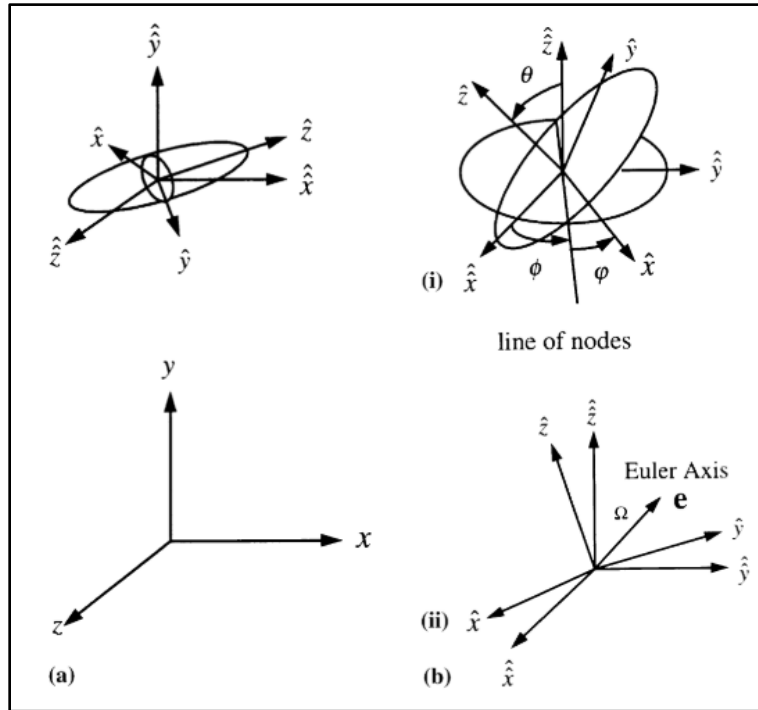


**Figure 5:** Clockwise from top left: Diagram of a prolate ellipsoid particle labeled with the inertial frame of reference  $(\hat{x}, \hat{y}, \hat{z})$  and the body frame of reference  $(\hat{x}, \hat{y}, \hat{z})$  which is aligned to the semimajor axis of the ellipsoid and centered at the particle centroid. The Euler angles between the inertial and body frame of reference are shown in the top right. The world frame of reference  $(x, y, z)$  is shown in the bottom left. The Euler's four parameters which are used to derive quaternion components is shown on the bottom right [14].

The inertial frame of reference is always aligned with the world frame of reference and centered at the particle centroid. The body frame of reference is aligned to the semimajor axis of the ellipsoid and centered at the particle centroid. The world frame of reference is fixed to the domain. The four Euler parameters are derived from the Euler angles and is seen in the bottom right of Figure 5 where the quaternion components are constrained by definition as:

$$\varepsilon_1^2 + \varepsilon_2^2 + \varepsilon_3^2 + \eta^2 = 1 \quad (\text{Eq. 27})$$

The transformation between the co-moving body frame of reference to the world frame of reference is given by the linear relations below:

$$\text{Vector:} \quad x = A^{-1}x^b \quad (\text{Eq. 28})$$

$$\text{Matrix:} \quad X = A^{-1}X^bA \quad (\text{Eq. 29})$$

where  $A$  is the transformation matrix. It is derived from the quaternion components:

$$A = \begin{bmatrix} 1 - 2(\varepsilon_2^2 + \varepsilon_3^2) & 2(\varepsilon_1\varepsilon_2 + \varepsilon_3\eta) & 2(\varepsilon_1\varepsilon_3 + \varepsilon_2\eta) \\ 2(\varepsilon_1\varepsilon_2 + \varepsilon_3\eta) & 1 - 2(\varepsilon_3^2 + \varepsilon_1^2) & 2(\varepsilon_2\varepsilon_3 + \varepsilon_1\eta) \\ 2(\varepsilon_1\varepsilon_3 + \varepsilon_2\eta) & 2(\varepsilon_3\varepsilon_2 - \varepsilon_1\eta) & 1 - 2(\varepsilon_1^2 + \varepsilon_2^2) \end{bmatrix} \quad (\text{Eq. 30})$$

After each integration of a quaternion, it is renormalized to unity through the following equation:

$$\varepsilon_i = \frac{\varepsilon_i}{\sqrt{\varepsilon_1^2 + \varepsilon_2^2 + \varepsilon_3^2 + \eta^2}} \quad (\text{Eq. 31})$$

Quaternions have the benefit of avoiding gimbal lock, faster computation time, and nonsingular representation (Zhao).

## 2.4 Simulation Program

A computer program was developed and written in MATLAB software to solve for the translation and rotation of an ellipsoidal particle under a customizable set of flow and particle parameters. The two explored flows include the Taylor-Green vortex flow which has an analytical solution as well as a fixed turbulent flow. The dynamics of the particles were calculated through the following major steps:

1. Initial particle parameters and fluid parameters are set manually to model the desired system. The computational domain is also set during this step with the desired domain in the Taylor-Green vortex flow. The computational domain in the turbulent three-dimensional flow is set as  $63^3$ .
2. Initial particle position, orientation, velocity, and angular velocity are specified.
3. The quaternion for the particle is then calculated from the orientation using the function `eul2quat()` [15].

4. The fluid velocity at the particle centroid and velocity gradient tensor at the particle centroid are calculated analytically in the Taylor-Green vortex flow and with central differencing in the three-dimensional turbulent flow.
5. The program then utilizes the quaternion and Equation 29 to generate rotation matrices for the fluid velocity gradient tensor and fluid velocity vector to generate resistance and velocity gradient matrices (Eq. 22-23) in the body frame of reference.
6. Newton's second equation of motion and the hydrodynamic torque and drag equations are integrated using an implicit forward Euler scheme over the timestep to determine the updated position and orientation of the particles.
7. The simulation returns to step three after recalculating the updated quaternion and position and loops until the simulation is terminated.
8. Data sets are saved after simulation runs to generate Figures 7-14.

## 2.5 Experiment Parameters

To determine the effects of anisotropic geometry on particle dynamics, simulations were conducted for particles with parameters from Table 1.

**Table 1:** Particle parameters for each particle type simulated. Particle aspect ratio was the primary experimental variable and was normalized across an equal mass of  $5 \mu g$ .  $\rho_p$  is also held constant at  $120 \text{ kg/m}^3$ .

Shape	Mass (kg)	$\lambda$	Semi-major axis ( $\mu\text{m}$ )	Semi-minor axis ( $\mu\text{m}$ )
Sphere	$5 \cdot 10^{-9}$	1.001	215.2	215.0
Ellipsoid	$5 \cdot 10^{-9}$	1.5	281.9	187.9
Ellipsoid	$5 \cdot 10^{-9}$	3	447.3	149.1
Ellipsoid	$5 \cdot 10^{-9}$	5	629.0	125.8
Ellipsoid	$5 \cdot 10^{-9}$	10	998.2	99.8
Ellipsoid	$5 \cdot 10^{-9}$	25	1838.8	73.6

For each of the parameters in Table 1 a simulation was ran for the Taylor-Green vortex flow and the three-dimensional turbulent flow. The Lagrangian simulation recorded all data from each time

step.  $\lambda = 1.001$  was selected rather than  $\lambda = 1$  to use the same equation set and to avoid running into unity errors. An aspect ratio of 1.001 is a frequently used value in the literature in regard to representing a sphere like object [11].

In the Taylor-Green vortex flow simulations, the particle began at the arbitrary starting position of  $x = 0.2$  and  $y = 0.2$ . In the three-dimensional turbulent flow simulations. The particle began at the starting position of  $x = 1$ ,  $y = 0$ , and  $z = 0$ . In both cases, the particles had an initial velocity matching the fluid velocity at the centroid, no angular velocity, and initial orientation of 0 rad in all Euler angle directions. The simulation ran until the particle reached a steady state within the flows. The flows had the same fluid parameters as described in Section 2.2.2.

### 3. Verification

To verify the time step error behavior of the simulation, the scheme was run for a particle of  $\lambda = 3$  and  $\rho_p = 120$  for the ellipsoidal particle in the Taylor-Green vortex flow. The root mean square error of the resting point of the ellipsoidal particle is calculated for time steps between 0.0025 and 0.0000375 and plotted on a logarithmic plot to verify if the error quantification is first order.

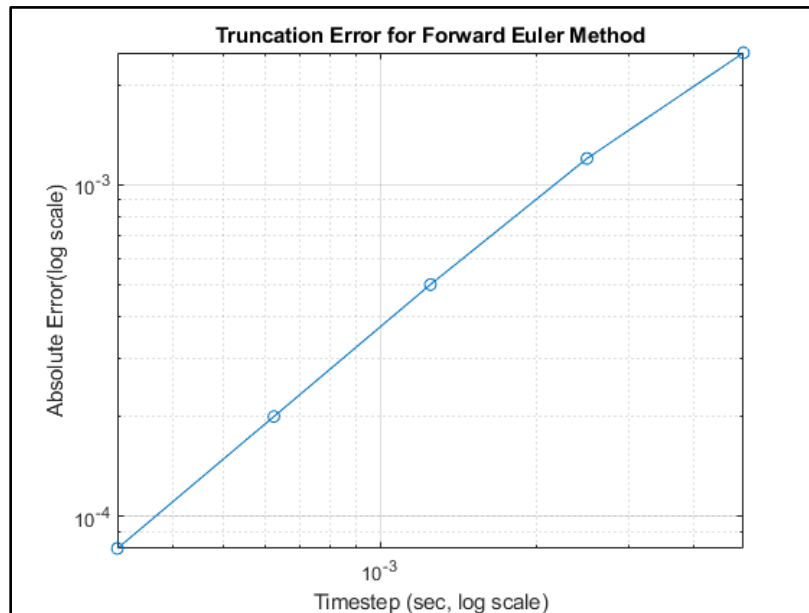


**Figure 6:** Figure showing the absolute error in average absolute deviation from true location for different time steps. First order error behavior is expected and verified in this figure with linear error.

Figure 6 confirms the first order error where absolute error of particle position is linear with timestep increase and was used to determine the applicable timestep in the simulations ran for the data presented in Section 4.

### 3.1 Validation

To determine the validity of the solver, simple test cases were used and compared to known behaviors. The first behavior tested was a sphere dropping through still viscous fluid under gravity. The terminal velocity reached in the simulation was compared to an analytical equation. The terminal velocity behavior of the sphere was calculated using the following equation:

$$v = \frac{2(\rho_p - \rho_f)}{9\mu} gR^2 \quad (\text{Eq. 32})$$

As the governing equations are the same between Equation 32 and the solver, the terminal velocity reached was identical. However, there was only very slight change in the time to reach terminal velocity due to the truncation error resulting from the first order approximation. Additionally, the solver also simulated spheres of varying diameters to validate that terminal velocity decreased at a square rate with an increase of radius.

## 4. Results & Discussion

Section 4 presents data produced by the solver simulating particles with parameters from Table 1 in both Taylor-Green vortex flow and the turbulent three-dimensional flow pictured in Figure 4. The two-dimensional laminar Taylor-Green vortex flow is presented first as it provides a simpler case to draw conclusions from. The three-dimensional turbulent flow simulation results are presented in section 4.2. In each section the velocity dynamics and orientation dynamics of particles of different aspect ratios are presented and discussed.

### 4.1 Taylor-Green Vortex Flow

Figure 7 through Figure 14 are generated by placing a single particle with one of the parameter cases from Table 1. In each simulation, the steps from section 2.5 were ran to collect data for a particle starting at the starting position of  $x = 0.2$  and  $y = 0.2$ . The simulation ran until the particle reached a steady state within the flow.

### 4.1.1 Translation Dynamics

For each particle case presented in Table 1 the velocity of the particle in the x and y directions was calculated. The magnitude of the particle velocity during the first five seconds of the flow is presented in Figure 7.

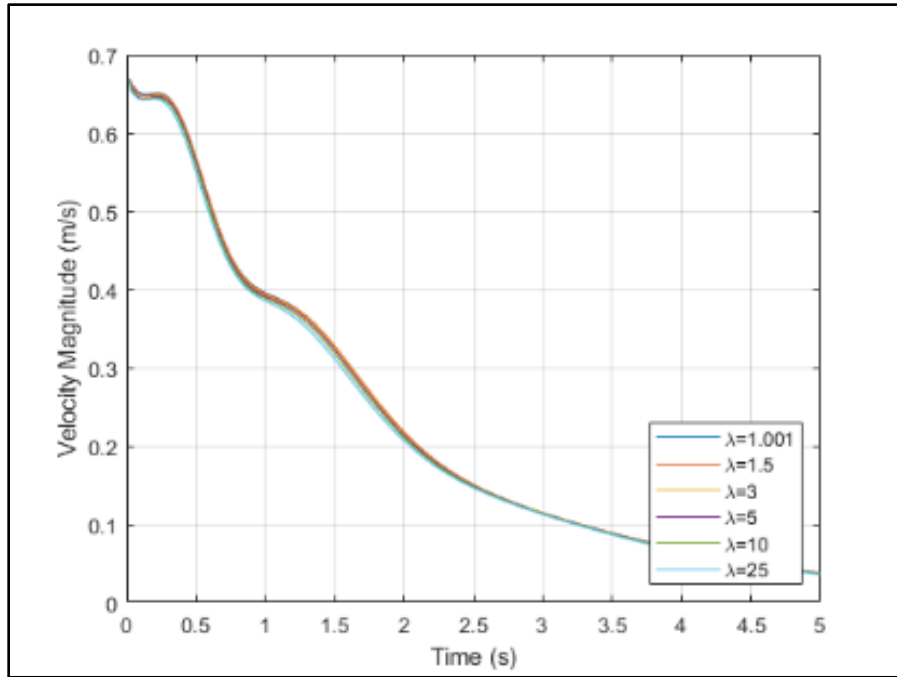


**Figure 7:** Average velocity magnitude for ellipsoidal particles in Taylor-Green vortex flow with aspect ratios from Table 1.

Each of the plotted velocity magnitudes for the particles followed a similar trajectory that began at the local fluid velocity and decayed as described in the Taylor-Green vortex flow equations. The decay of the particle velocities is not constant and has identifiable points where the slope of velocity decrease changes. This is explained by two phenomena. The first behavior is the particle moving towards the outer part of the vortex due to the uneven centripetal and centrifugal forces placed on the particle flow at its initial position and velocity. As the forces are balanced through particle mass primarily, the particles having the same overall translational behavior is expected. In addition, this movement to the outer part of the vortex may explain the shape of the decay in velocity magnitude. The second substantial force resulting in this behavior is the initial rotation of the particle. During the initial phase of the simulation the major axis of the prolate ellipsoid rotates to better align with the stream wise direction to equalize the hydrodynamic torques placed on the

particle. The varying change in orientation of the particle relative to the streamwise direction results in slight variations to the particle velocity magnitude which explains the minor differences between the six particle aspect ratios simulated. Figure 8 presents the difference in velocity between each of the particles more clearly by comparing the difference between particle velocity magnitudes and fluid velocity magnitudes.

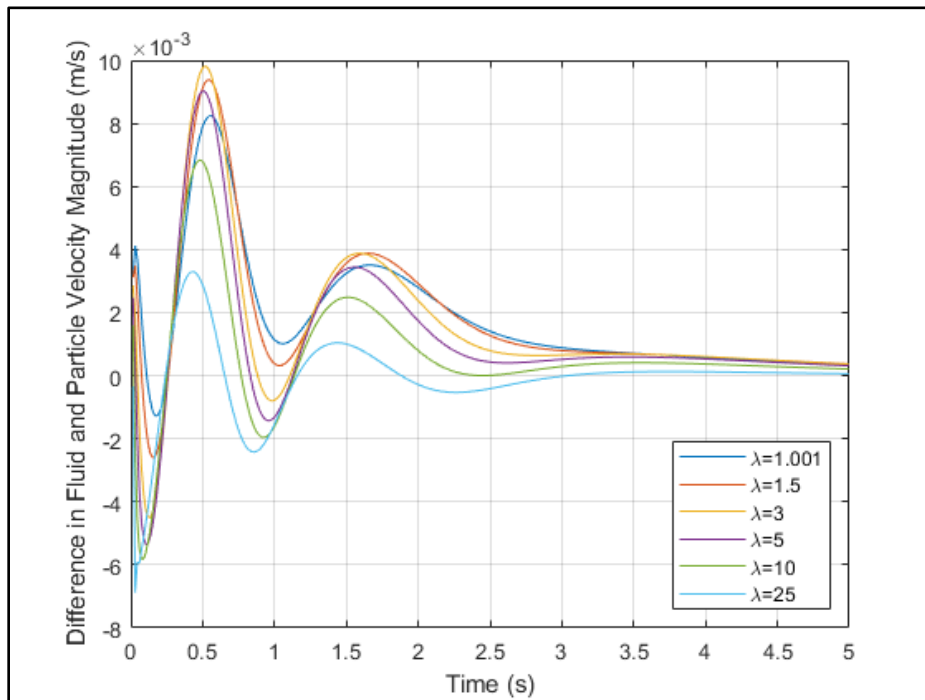


**Figure 8:** The difference between the velocity magnitude of the particle and the fluid velocity at the particle centroid.

The data presented in Figure 8 shows that between the particle and the fluid there was some differential velocity before settling after rotation had largely stopped. Each of the different aspect ratio particles showed a unique difference for each time point. Generally, the trend shows that higher aspect ratio particles were quicker to reach the steady state fluid velocity than the lower aspect ratio particles. This can be explained by the longer moment arms of the particle major axis being affected more strongly by hydrodynamic torque to shed angular velocity more quickly than the lower aspect ratio particles. Of the six particle aspect ratios simulated, the particle with  $\lambda = 3$  had the greatest velocity differential. Between the  $\lambda = 3$  and  $\lambda = 1.001$  particle there was a

reduction in peak velocity differential indicating that the specific particle and fluid parameters result in a particle with an aspect ratio between 1.5 and 5 having the greatest velocity differential.

#### 4.1.2 Orientation Dynamics

In this section the orientation dynamics from the same simulation as ran in Section 4.1.1 are presented. Figure 9 presents the angular velocity of each of the six particles placed in the Taylor-Green vortex flow.

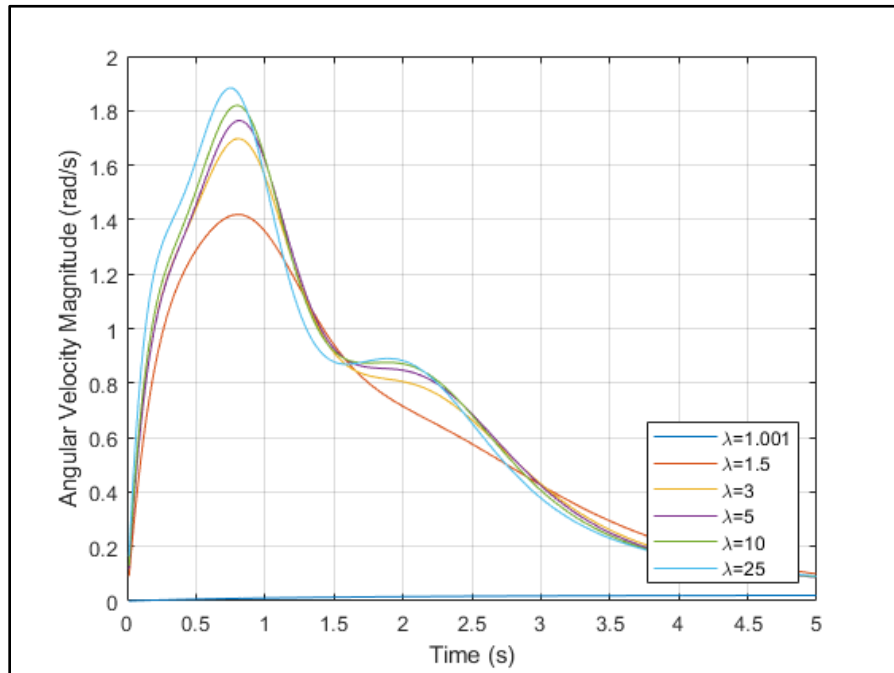


**Figure 9:** Average angular velocity for ellipsoidal particles in Taylor-Green vortex flow with parameters presented in Table 1.

The results presented in figure 9 indicate that the average angular acceleration correlated with aspect ratio. The  $\lambda = 25$  particle has the greatest peak angular velocity when all particles start at the same initial position, orientation, velocity, and angular velocity. The  $\lambda = 1.001$  particle exhibits almost no change in angular velocity and is a result of the nearly spherical shape not being affected by the hydrodynamic torque. There is some angular velocity in the  $\lambda = 1.001$  particle likely because of the shear forces acting on the sides of the particle. This positive correlation between aspect ratio and angular acceleration magnitude is a result of the larger moment arms at equivalent masses for higher aspect ratio particles. These moment arms increase the effects of

hydrodynamic torque relative to the moment of inertia for each particle. The positional values for each of the particles during the simulations is presented in Figure 10.

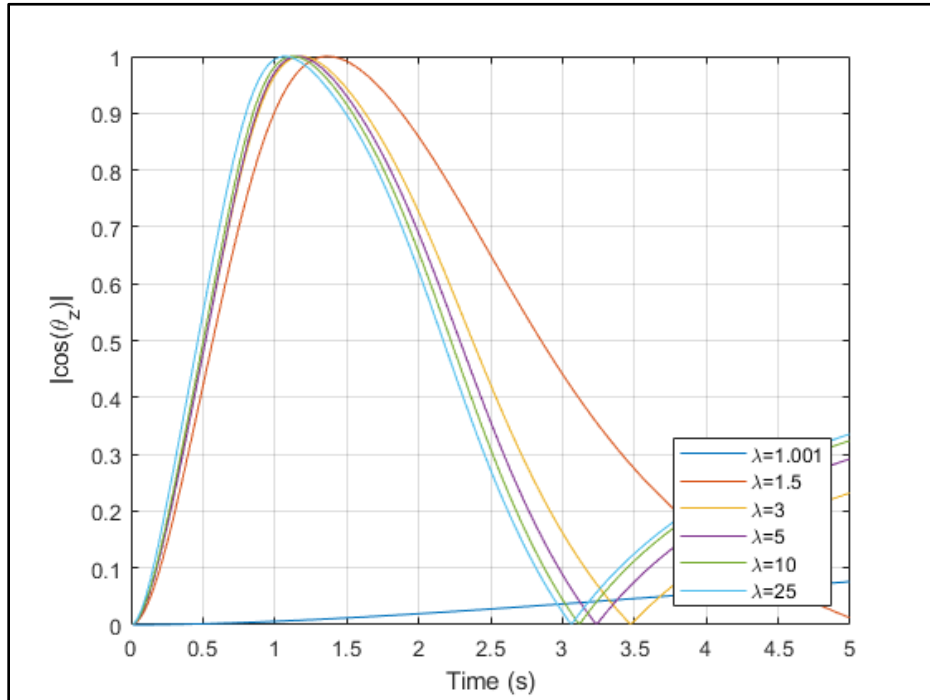


**Figure 10:** Absolute value of the particle direction cosine between the semimajor axis and world z axis as seen in Figure 1 for ellipsoidal particles in Taylor-Green vortex flow with parameters presented in Table 1.

The results presented in Figure 10 reinforce the discussion points from the prior paragraph as the higher aspect ratio particles have a faster rate of angle change during each simulation. The  $\lambda = 1.001$  particle exhibits different behavior here due to the minimal hydrodynamic torque. Additionally, the slowing rate of angular velocity over time for all the particles seen in Figure 10 is also reflected in Figure X by the direction cosine flattening out over time.

### 4.1.3 Particle Energy

The velocity data presented in Figure 7 and Figure 9 was combined to find the total kinetic energy of the particle in each simulation and is presented in Figure 11.

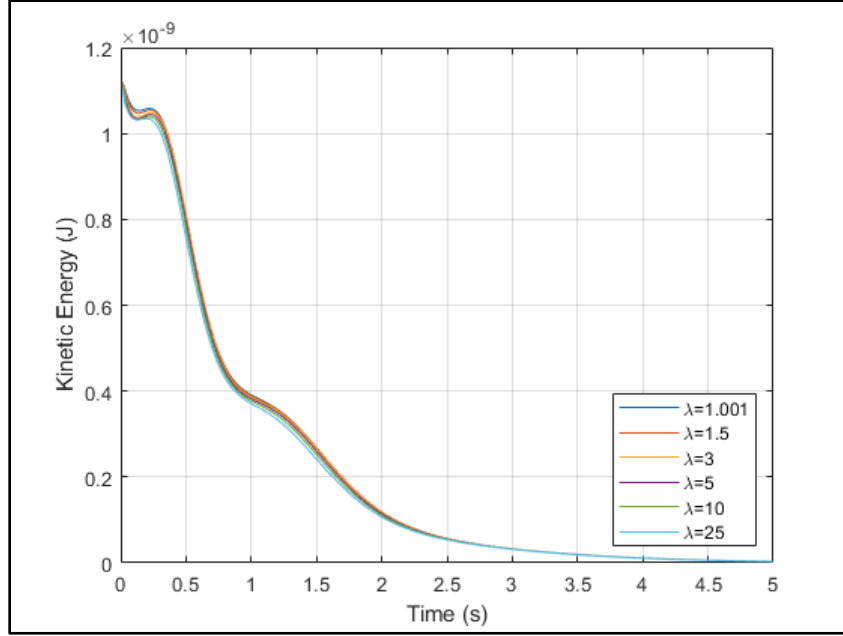


**Figure 11:** The total kinetic energy of each particle over time with differing aspect ratios when placed in Taylor-Green vortex flow.

The total kinetic energy was calculated using the following two equations:

$$K.E. = \frac{1}{2}mv_p^2 + \frac{1}{2}I_p * \omega^2 \quad (\text{Eq. 33})$$

where,

$$I_p = \frac{1}{5}m(a^2 * c^2) \quad (\text{Eq. 34})$$

The data presented in Figure 11 further supports the explanation of particle aspect ratio having minimal affect on translational behavior when the particle has equivalent masses. While there is some variance between particles in total kinetic energy due to the rotational component, the majority of kinetic energy comes from the particles translational motion and closely mirrors the change in particle translational velocity.

## 4.2 Turbulent Flow Dynamics

Section 4.2 presents the dynamics data for the solver simulating ellipsoidal particles of varying aspect ratios in the three-dimensional turbulent flow presented in Figure 4. The same procedure was used, as in Section 4.1, where a single particle was placed in the flow and tracked. Each

particle started with no initial velocity or angular velocity and began at the position of  $x, y, z = 0, 0, 0$ . The simulation ran until the particle reached the domain boundary. Particle translational velocity data and overall kinetic energy were calculated and are presented in Figure 12 through Figure 14. The orientation dynamics figures are not present as they quickly diverge and do not offer conclusions to draw from. This is likely due to the coarse grid size of 63 units on each axis with the particles quickly changing rotation rates too quickly. To get useful conclusions, a different analysis would be needed for the particles in 3D flow where many particles are simulated, and statistics are collected using nondimensional analysis. The velocity magnitude was calculated and is presented in Figure 12.

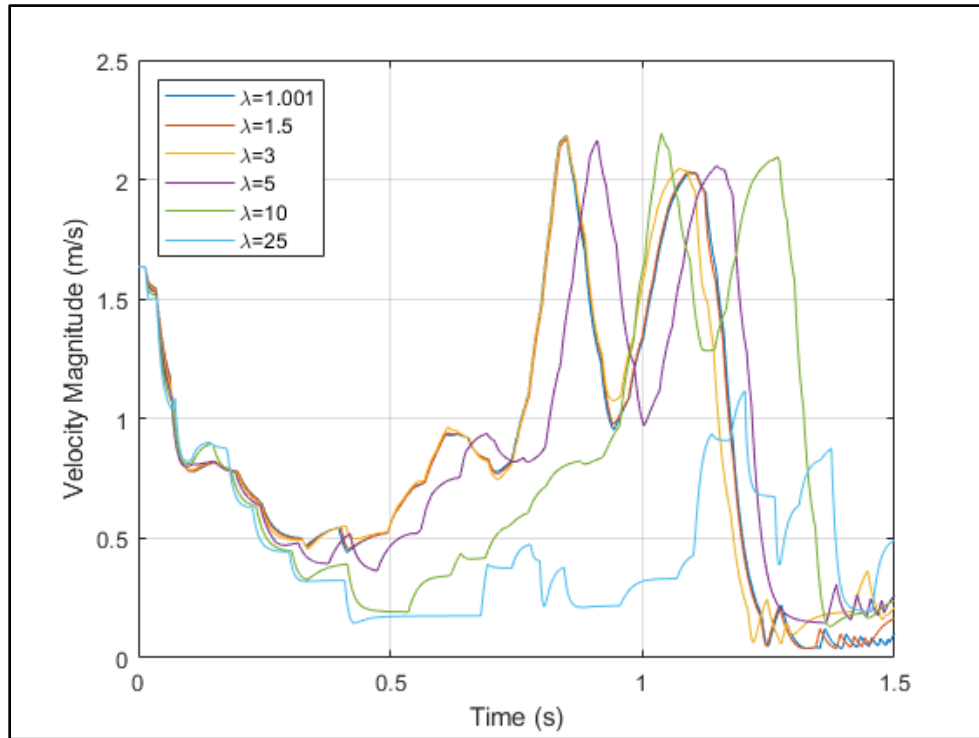


**Figure 12:** Average velocity magnitude for ellipsoidal particles in three-dimensional turbulent flow with aspect ratios from Table 1.

The velocity data presented in Figure 12 shows that while the particles begin with the same velocity and trajectory, they quickly begin to deviate within 0.5 seconds. This behavior is expected as the turbulent three-dimensional flow has significantly different shear forces acting on a particle based on its location. Slight changes in position in the three-dimensional domain have significantly

different velocity values and velocity gradients. The smaller aspect ratio particles are seen in this figure to be able to traverse the domain at a faster velocity overall than the particles with higher aspect ratios. This could be explained by the higher local velocity differentials in the fluid presented in Figure 13. This figure shows that like in Figure 8 the particles with higher aspect ratios are less affected by the velocity of the fluid at the center of the particle and had more relative hydrodynamic torque effects.

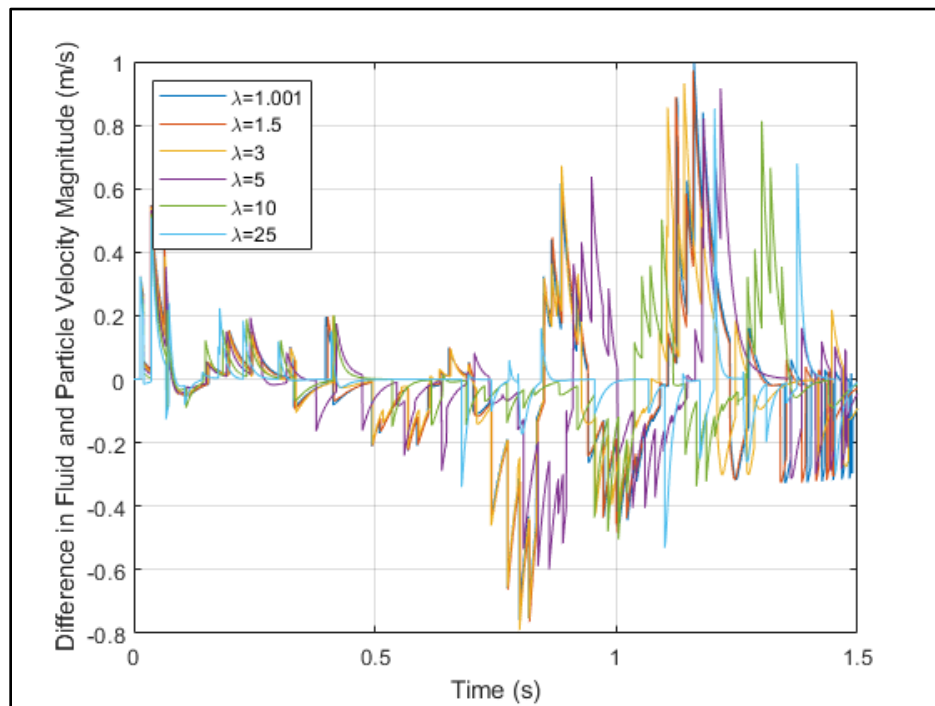


**Figure 13:** The difference between the velocity magnitude of the particle and the fluid velocity at the particle centroid.

The differential velocity between the fluid and particle shows messier data which gives insight on the effects of the coarse grid size on the particle and the single order central differencing formula used to calculate the velocity and velocity derivatives at each particle centroid. The kinetic energy over time for each particle was also plotted in Figure 14.

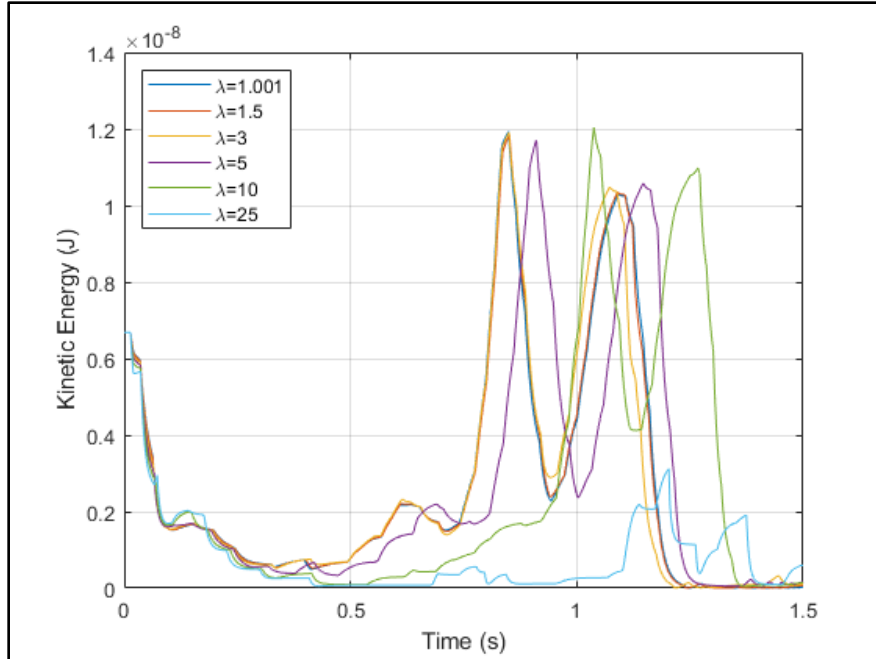


**Figure 14:** The total kinetic energy of each particle over time with differing aspect ratios when placed in Taylor-Green vortex flow.

The kinetic energy of the particle mirrors the velocity data closely with a key difference being the particle with the aspect ratio of 25 having a lower relative energy throughout the data set than the other particles. This could be due to the  $\lambda = 25$  particle having a lower average velocity than the other particles thus a lower average angular velocity. The angular velocity seems to be higher when the particle is moving faster translationally.

## 5. Conclusion

In this thesis, the rationale and methods used to create a solver for simulating anisotropic ellipsoidal particles suspended in flows was presented. The kinematics and dynamics equations, as well as the solver logic was explained to show how the Lagrangian tracking of particles was possible. Data collected from the solver simulating particles of varying aspect ratios was then presented for both a two-dimensional laminar flow and three-dimensional turbulent flow to show its capabilities. Overall, the solver can successfully simulate anisotropic particles in varying fluid flow and particle parameters resulting in meeting the research objective of this work. The simulations ran in the solver resulted in notable takeaways that should be further substantiated in the future. The simulations showed that in the laminar case, the particles tended to orient in the

stream wise direction and that settling orientation speed correlated with higher aspect ratios. This was explained to be due to the greater hydrodynamic torques acting on the particle due to the greater moment arms of large major axis particles. This behavior is also reflected in the kinetic energy graphs of the three-dimensional turbulent flow simulation. For the translational behavior of the particles, the laminar case showed only minor change in translational velocity with changing aspect ratio. Particles with lower aspect ratios tended to have a lower average difference between the particle and fluid velocity. This can be explained through the greater surface area to mass ratio of the particle thus being more affected by the viscous forces of the fluid and thus slowing down faster with less inertial effects. The three-dimensional turbulent flow showed that ellipsoidal particles can quickly divert based on aspect ratio but loosely supports the same conclusions as the laminar 2D case where rounder particles are able to traverse the domain faster.

## **5.1 Next Steps**

The solver presented in this work can be used to further explore anisotropic particle behavior by comparing particles of different parameters such as particle density to fluid density ratio, oblate ellipsoids, higher aspect ratios, and intermediate aspect ratios. In addition, other flows can be used when analyzing particles. The solver could be improved by adding capabilities to simulate flows with rigid boundary conditions such as channel flow. The solver can also be improved by moving to two-way coupling (fluid affects particles, particles affect fluid) or four-way coupling (domain boundary affects particles, particles affect particles). In addition, the accuracy of the current solver can be improved at the cost of computational expense by moving to higher order Runge-Kutta methods and differencing equations than the forward Euler and central differencing methods used in this simulation. Finally, to draw more conclusive data from the turbulent three-dimensional flow it would be possible to simulate many more particles with the same particle parameters and to collect statistics rather than track individual particle trajectories.

## References

- [1] Pakseresht, Pedram, and Apte, Sourabh V. “Modeling the Dense Spray Regime Using an Euler-Lagrange Approach With Volumetric Displacement Effects” 2019.
- [2] Paschkewitz, J. S, et al. “Numerical Simulation of Turbulent Drag Reduction Using Rigid Fibres.” *Journal of Fluid Mechanics*, vol. 518, 2004, pp. 281–317.
- [3] Computational Flow Physics Laboratory: Sourabh Apte Research Group, [web.engr.oregonstate.edu/~sva/](http://web.engr.oregonstate.edu/~sva/).
- [4] Mortensen, P.H, et al. “On the Orientation of Ellipsoidal Particles in a Turbulent Shear Flow.” *International Journal of Multiphase Flow*, vol. 34, no. 7, 2008, pp. 678–683.
- [5] Parsheh, Mehran, et al. “On the Orientation of Stiff Fibres Suspended in Turbulent Flow in a Planar Contraction.” *Journal of Fluid Mechanics*, vol. 545, no. 1, 2005, pp. 245–269.
- [6] Paschkewitz, J. S, et al. “An Experimental and Numerical Investigation of Drag Reduction in a Turbulent Boundary Layer Using a Rigid Rodlike Polymer.” *Physics of Fluids (1994)*, vol. 17, no. 8, 2005, p. 85101.
- [7] Jeffery, George Barker. “The Motion of Ellipsoidal Particles Immersed in a Viscous Fluid.” *Proceedings of the Royal Society of London. Series A, Containing Papers of a Mathematical and Physical Character*, vol. 102, no. 715, 1922, pp. 161–179.
- [8] Brenner, H. “The Stokes Resistance of an Arbitrary Particle—III: Shear Fields.” *Chemical Engineering Science*, vol. 19, no. 9, 1964, pp. 631–651.
- [9] Chang, I.-D, and Harper, E. Y. *Maximum Dissipation Resulting from Lift in a Slow Viscous Shear Flow*, 1968.
- [10] Zhao, F, and Van Wachem, B G. M. “Direct Numerical Simulation of Ellipsoidal Particles in Turbulent Channel Flow.” *Acta Mechanica*, vol. 224, no. 10, 2013, pp. 2331–2358.
- [11] Zhang, Haifeng, et al. “Ellipsoidal Particles Transport and Deposition in Turbulent Channel Flows.” *International Journal of Multiphase Flow*, vol. 27, no. 6, 2001, pp. 971–1009.
- [12] Voth, Greg A, and Soldati, Alfredo. “Anisotropic Particles in Turbulence.” *Annual Review of Fluid Mechanics*, vol. 49, no. 1, 2017, pp. 249–276.
- [13] "File:Ellipsoid-rot-ax.svg." Wikimedia Commons, the free media repository. 28 Oct 2020, 02:25 UTC. 4 Jun 2021, 18:59.
- [14] Marchioli, Cristian, et al. “Orientation, Distribution, and Deposition of Elongated, Inertial Fibers in Turbulent Channel Flow.” *Physics of Fluids (1994)*, vol. 22, no. 3, 2010, p. 33301.

[15] “eul2quat: Convert Euler Angles to Quaternion.” *Convert Euler Angles to Quaternion - MATLAB*, [www.mathworks.com/help/robotics/ref/eul2quat.html](http://www.mathworks.com/help/robotics/ref/eul2quat.html).

